J Electron Test (2015) 31:85–98
DOI 10.1007/s10836-015-5505-9

Low Cost Sparse Multiband Signal Characterization Using Asynchronous Multi-Rate Sampling: Algorithms and Hardware

Nicholas Tzou · Debesh Bhatta · Barry J. Muldrey Jr. · Thomas Moon · Xian Wang · Hyun Choi · Abhijit Chatterjee

Received: 25 September 2014 / Accepted: 7 January 2015 / Published online: 30 January 2015

Abstract Characterizing the spectrum of sparse wideband signals of high-speed devices efficiently and precisely is critical in high-speed test instrumentation design. Recently proposed sub-Nyquist rate sampling systems have the potential to significantly reduce the cost and complexity of sparse spectrum characterization; however, due to imperfections and variations in hardware design, numerous implementation and calibration issues have risen and need to be solved for robust and stable signal acquisition. In this paper, we propose a low-cost and low-complexity hardware architecture and associated asynchronous multi-rate sub-Nyquist rate sampling based algorithms for sparse spectrum characterization. The proposed scheme can be implemented with a single ADC or with multiple ADCs as in multi-channel or band-interleaved sensing architectures. Compared to other sub-Nyquist rate sampling methods, the proposed hardware scheme can achieve wideband sparse spectrum characterization with minimum cost and calibration effort. A hardware prototype built using off-the-shelf components is used to demonstrate the feasibility of the proposed approach.

Keywords Asynchronous multi-rate sampling · Low cost spectrum sensing and characterization · Sub-Nyquist rate sampling

1 Introduction

To transfer data at higher data rates, RF and digital signals are pushed to operate across wider bandwidths. In many measurement systems, characterizing the spectral content of these wideband signals with ADCs is critical for assessing the performance of the underlying electronics but becomes difficult as well as expensive for multi-GHz signals at Nyquist sampling rates. Signals with sparse representations in the frequency domain can be to recovered with sub-Nyquist sampling. Numerous sub-Nyquist sampling schemes have been studied and applied to sparse wideband spectrum characterization. In the past, compressive sensing algorithms have been used to recover signals with fewer samples [3, 5, 23]. Modulated wideband converters (MWC) [17, 18] and random demodulation [12, 14, 20] involve mixing wideband input signals with a multi-tone signal containing spectral components across the entire input bandwidth. Mixer non-linearity creates additional tones that reduce spectrum sparsity and can degrade the signal reconstruction performance. Mixing with a wideband multi-tone signal generates more intermodulation products and exacerbates the problem. What is needed is extensive calibration for delay and nonlinearity of the mixer, but this increases the overall cost of the system. Calibration plays an even more important role in synchronous multi-channel systems. For example, MWC and multi-coset sampling [2, 15, 16, 26] require precise delay synchronization across multiple channels and are susceptible to delay and sampling frequency variations. Uncertainties in these delays degrade the recovery performance of the associated algorithms [7]. Other algorithms have been proposed to compensate for timing mismatches, but these substantially increase the complexity of the receiver [6, 11]. Non-uniform sampling [27] and random sampling [13, 19] are techniques that use a custom designed ADC to collect fewer samples for signal reconstruction. However, they cannot operate beyond the maximum sampling rate of the designed ADCs, which limits the usability of the method for high-frequency signals. In [1, 4, 8–10, 21, 22], algorithms and hardware are described for acquiring signals using optical

Responsible Editor: S. Sunter

N. Tzou (✉) · D. Bhatta · B. Muldrey Jr. · T. Moon · X. Wang · H. Choi · A. Chatterjee
Georgia Institute of Technology, Atlanta, GA, USA
e-mail: nltzou@gmail.com

modulation and constant rate sampling, which mimic the effects of multi-rate sampling but are difficult to implement at low cost.

In this paper, we propose a low-cost asynchronous multi-rate sub-Nyquist sampling framework for characterizing signals that have a sparse spectrum. Multi-rate sampling can be subcategorized into asynchronous and synchronous multi-rate sampling. Compared to synchronous sampling, asynchronous multi-rate sampling does not require phase synchronization across different channels. This relaxes the associated hardware design cost and reduces the calibration effort. The proposed system is scalable because it can be implemented with a single channel or with multiple channels. In addition to the hardware design, associated algorithms are proposed to deal with the discrete spectrum and spectral grid mismatch. In this context, the Fast-Fourier Transform (FFT) is commonly used to convert time-domain samples into a vector in the frequency domain. However, when different sampling frequencies are used, the spectral grids of the vectors are not aligned, which makes it difficult to compare spectra from different sample sets corresponding to different sampling rates. A hardware prototype is built with off-the-shelf electrical components and measurements are taken to verify the architecture and algorithms proposed in this paper. The paper is organized as follows: Section II addresses the proposed spectrum sensing algorithms. Section III discusses the proposed hardware design. Section IV presents hardware measurement and verification results. Section V discusses conclusions.

2 Multi-Rate Spectrum Characterization

The proposed multi-rate sensing algorithm for wideband spectrum characterization is implemented using a two-step approach. The first step is to detect the input active bands, which are defined as the frequency bands containing significant input signal energy levels compared to that of the noise floor of the signal. High-resolution estimation of the frequency of the active bands is not required in this step; therefore, fewer samples are used to reduce the computational cost. The second step is to characterize the spectra of the detected active bands, and thus, more samples are used in this step to achieve higher frequency resolution.

2.1 Active Band Detection with Multi-Rate Sampling

Suppose a signal, band-limited to B, contains two active bands and is undersampled with two different sampling frequencies, F_{S1} and F_{S2}, as shown in Fig. 1. Because the sampling frequencies are different, each sample set has a different aliasing spectrum. By concatenating and comparing the aliasing spectra, we can determine the location of the active bands. The proposed active band detection algorithm is based on the concept of spectral comparison.

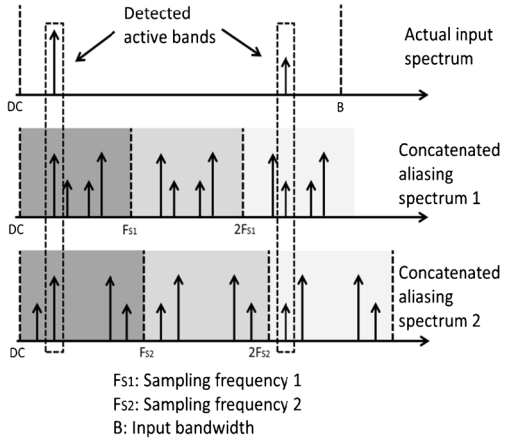

Fig. 1 Detecting active bands by comparing the aliasing spectra

Since the sampling frequencies are different, an immediate issue in comparing the spectra is that the spectral grids of FFT are different. A common frequency grid is needed to compare the aliasing spectra. As shown in Fig. 2, the signal is sampled with two sampling frequencies F_{S1} and F_{S2}. M samples are collected, and two sample sets, $\overline{y_1}$ and $\overline{y_2}$, are formed. The FFT spectral grid spacing for sample set 1 and 2 are F_{S1}/M and F_{S2}/M, which are not aligned. To form a common spectral grid, we divide the input bandwidth B into N equally spaced spectral grids, which is used to form one sensing matrix for each sample set. To preserve spectral information, B/N has to be less than or equal to F_{S1}/M and F_{S2}/M. The sensing matrices, A_1 and A_2, serve effectively as the Inverse Discrete Fourier Transform (IDFT) matrices. An IDFT matrix is associated with the sampling frequency and the sampling times of the collected samples. The sampling frequency is now determined by the spacing of the common spectral grid, B/N, and the sampling times are the sampling times of the samples denoted as ${t_1}^1$ to ${t_1}^M$ for sample set 1 and ${t_2}^1$ to ${t_2}^M$ for sample set 2 in Fig. 2. The aliasing spectra, as shown in Fig. 1, can be calculated by ${A_1}^H\overline{y_1}$ and ${A_2}^H\overline{y_2}$, where H represents the Hermitian transpose. In the following discussion, we refer to this common spectral grid, $\left[\frac{-NB}{2B}, \ldots, \frac{NB}{2B}\right]$, as the frequency support of the aliasing spectra.

We now use the following example to illustrate the proposed active band detection algorithm. As in Fig. 3, a two-tone signal is sampled with two different frequencies. The two aliasing spectra are shown in the first two spectra of Fig. 4. After the aliasing spectra are compared, the frequency support containing the highest energy level in both spectra can then be chosen to be the first active band. We then subtract, together with the corresponding negative frequency support of the first detected active band, the components of the first active band from the two time domain sample sets. The remaining

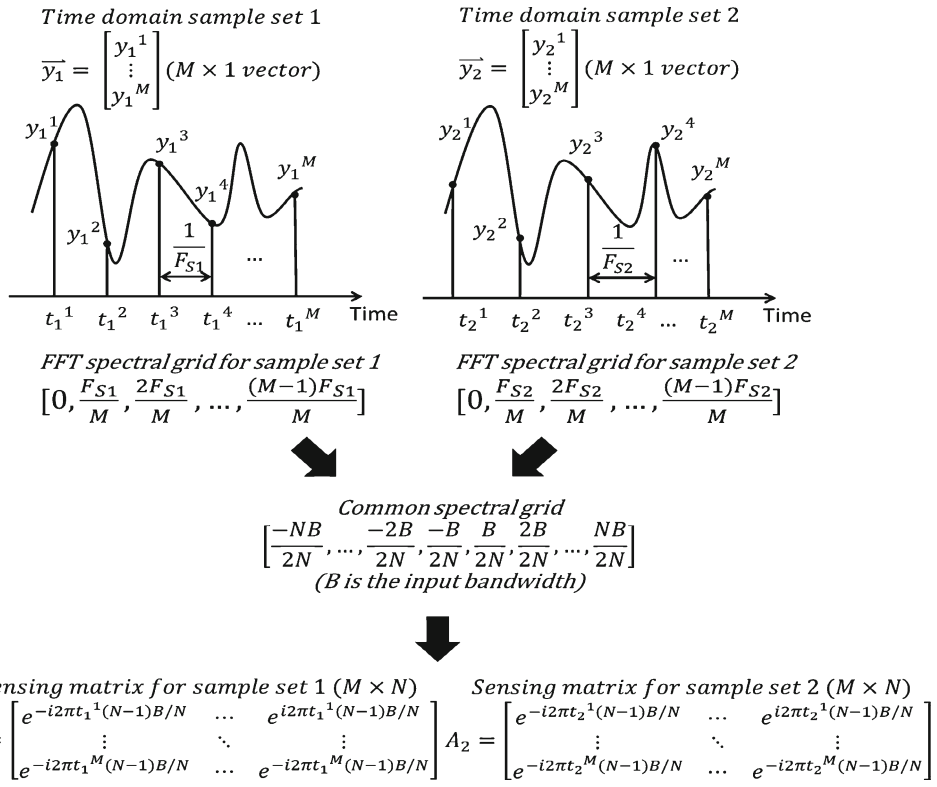

Fig. 2 Constructing a sensing matrix for each sample set using a common spectral grid (common frequency support)

waveforms are called the residual waveforms, $\overline{r_1}$ and $\overline{r_2}$, as shown in Fig. 5. We then calculate ${A_1}^H \overline{r_1}$ and ${A_2}^H \overline{r_2}$ to form the aliasing spectra of the residual waveform, as shown in Fig. 6. Next, we detect the frequency support of the second active band by comparing the two spectra. After subtracting the component of the second active band from the residual waveform, $\overline{r_1}$ and $\overline{r_2}$, we can see that the residual waveform after the second iteration is close to zero, as shown in Fig. 7. The proposed algorithm processes the samples and extracts the active bands iteratively. The stopping criteria of the algorithm is reached when the iteration reaches the number of the active bands (if the number of active bands is known), or when the energy of the residual waveform is below some predefined level. It is important to note that when we subtract the active band component from the time domain waveform, we do so for each sample set, instead of jointly for both. By doing so, the relative delays across different channels are not needed, reducing the effort needed for calibration and increasing the robustness of the signal acquisition system. The proposed algorithm is based on the Orthogonal Matching Pursuit (OMP) algorithm [24]. A flow chart of the proposed active band detection algorithm is shown in Fig. 8. As can be

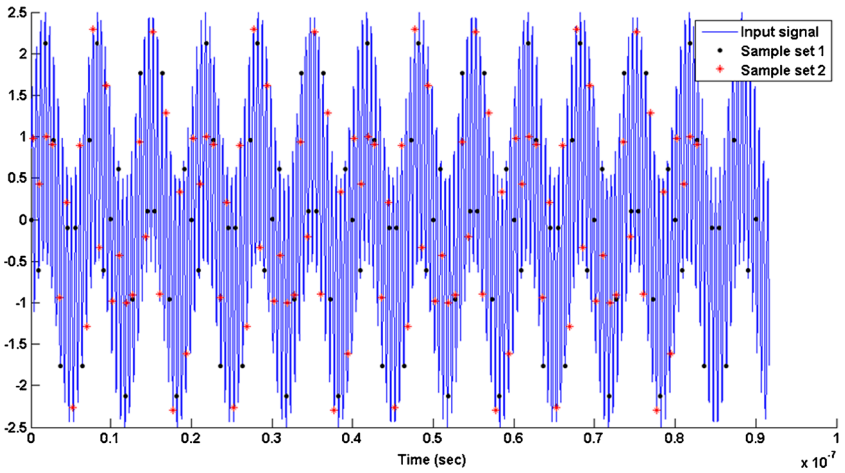

Fig. 3 Two tone signal sampled with two endiffert sampling frequencies

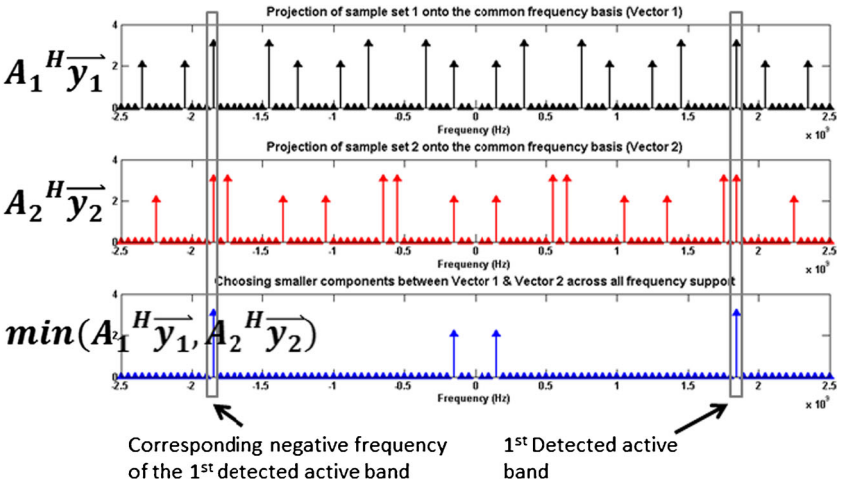

Fig. 4 Comparing two aliasing spectra to detect the active band (1st iteration)

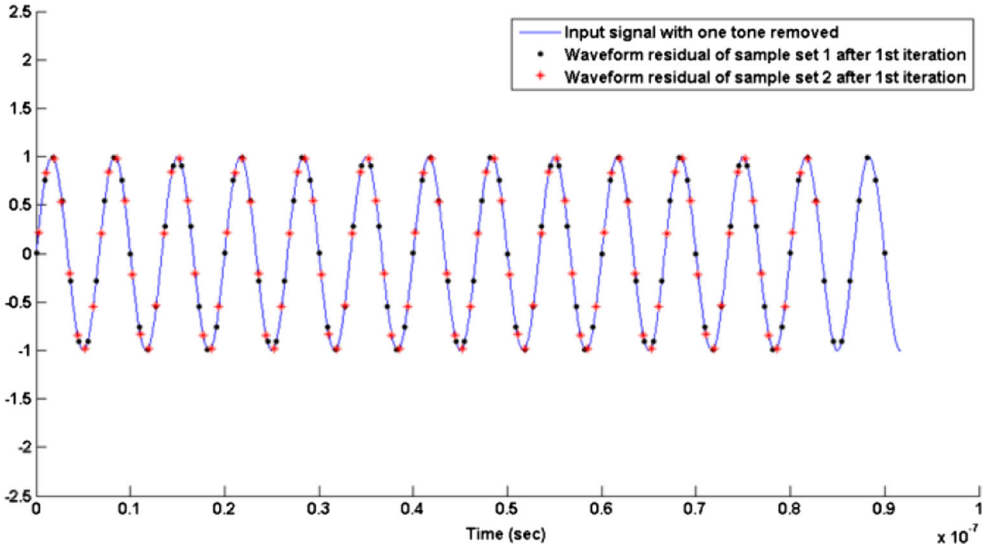

Fig. 5 Residual waveform after 1st iteration

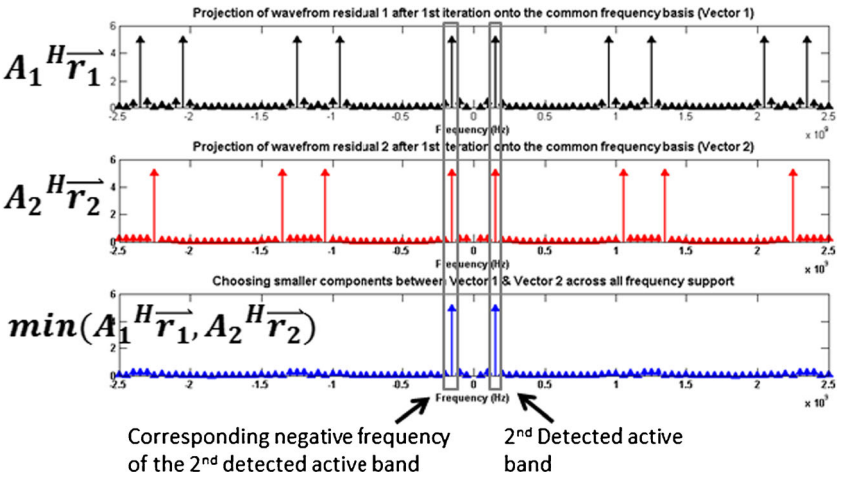

Fig. 6 Comparing two aliasing spectra to detect the active band (2nd iteration)

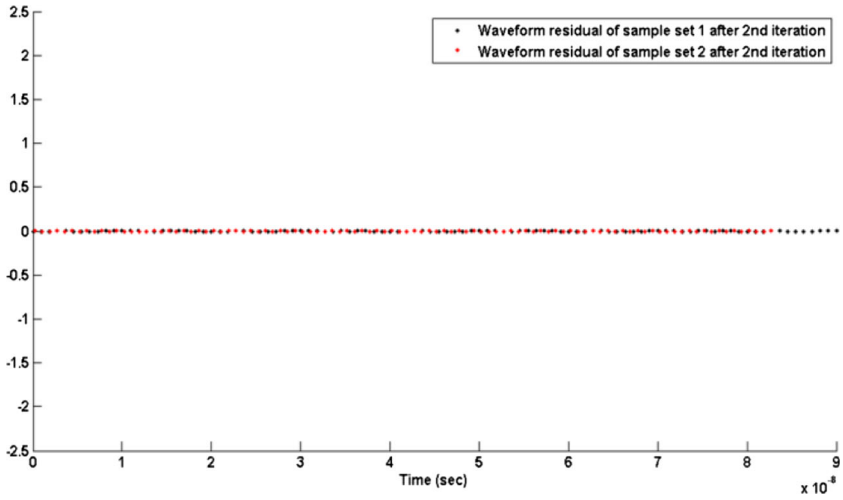

Fig. 7 Residual waveform after 2nd iteration

expected, if two active bands fall onto the same frequency support in the aliasing spectra, the algorithm may fail. Therefore, we perform analysis using simulation, to investigate how the signal reconstruction performance is impacted in terms of the probability of successful detection of multiple randomly selected active bands.

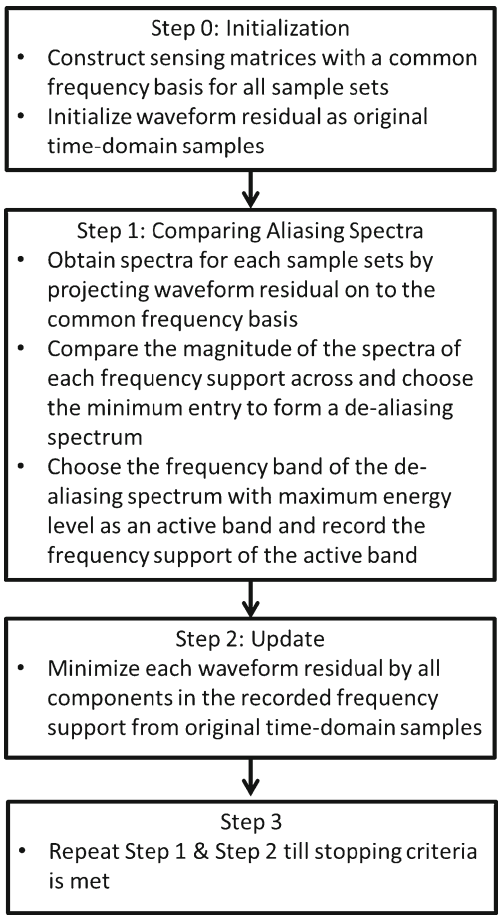

Fig. 8 Flow chart of the proposed active band detection algorithm

We use a two-tone signal and two-rate asynchronous sampling to explain the proposed algorithm. With the asynchronous scheme, the system can be easily scaled to multi-rate sampling. As we use more frequencies to sample the input signal, more sample sets are acquired. As can be seen from the Fig. 9a–c, as we increase the number of sample sets from 2 to 5, the number of successful detection in 100 runs increases. The other parameter in Fig. 9 is the input bandwidth. The proposed method relies on comparison of the aliasing spectra. As the input bandwidth is increased, we need to extend the aliasing spectra to cover the entire input bandwidth; thus, the probability of wrong detection increases. Therefore, the number of successful detections reduces, as shown in Fig. 9. The other parameter that affects the performance of signal reconstruction is the number of samples used in the detection. Spectra with higher resolution (larger numbers of samples) give better reconstruction performance. As can be seen in Fig. 10, we can increase the number of successful active band detections at the cost of increasing computation.

2.2 Active Band Spectrum Characterization

In the previous section, only relatively fewer samples, typically a few hundred samples, are used for detecting active bands. However, spectral resolution is directly related to the number of samples used for characterization; therefore, all the acquired samples are used in the spectrum characterization step. Since we characterize only the frequency support around the active bands, the computational cost is not as much.

Even with correct detection of the frequency support of the active bands, overlapping of active bands can occur in some sample sets. Therefore, an algorithm is needed to select only one sample set for spectral characterization of each detected active band. We will explain the proposed spectrum characterization algorithm with an example in the next paragraph.

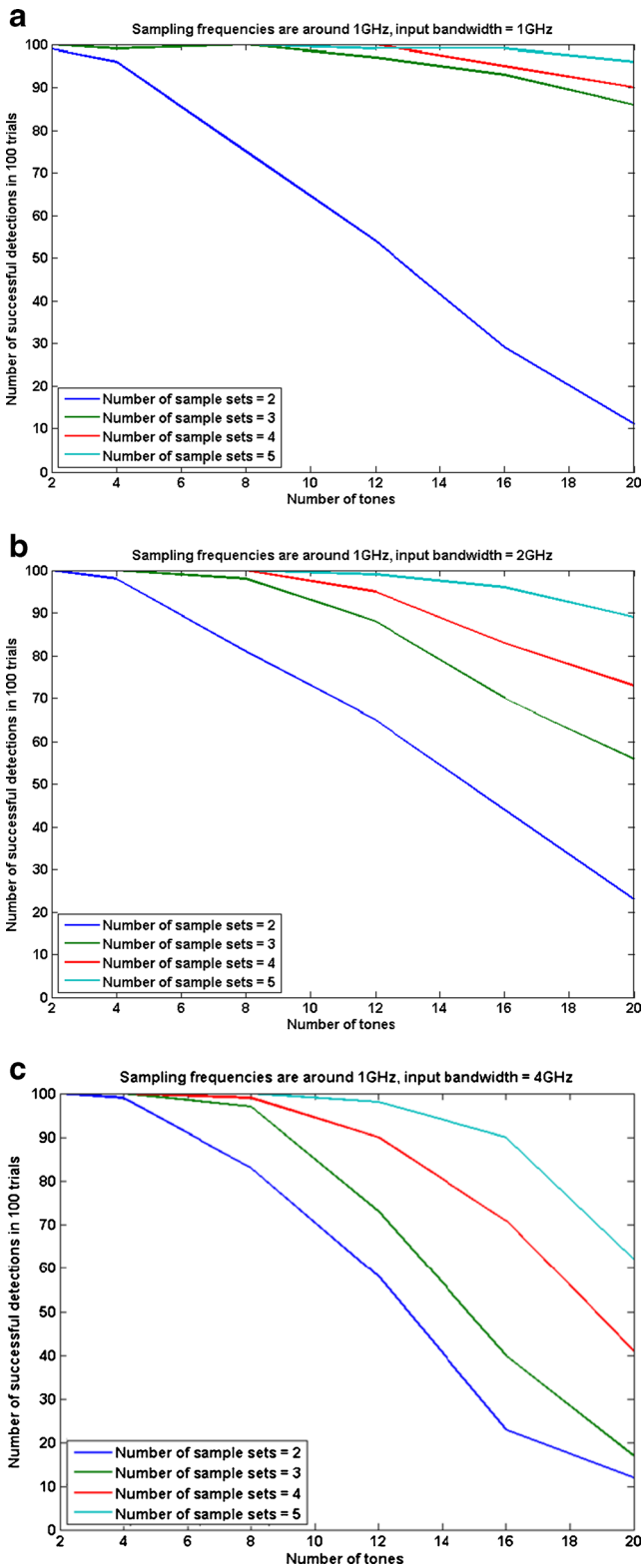

Fig. 9 **a** Reconstruction performance with 1GHz input bandwidth. (X-axis: number of randomly selected tones, Y-axis: number of successful reconstruction in 100 trials) **b** Reconstruction performance with 2GHz input bandwidth. **c** Reconstruction performance with 4GHz input bandwidth

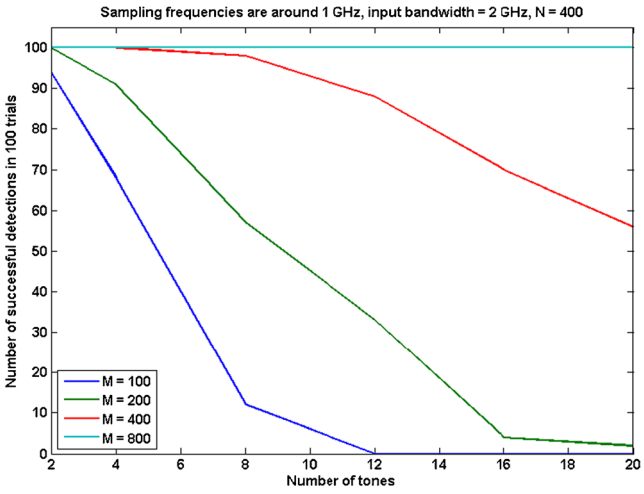

Fig. 10 Reconstruction performance increases as the number of samples increases

Suppose three 30-MHz bandwidth channels are chosen randomly from the 5GHz band to form the input signal. In this simulation, the randomly chosen center frequencies of each active channel are 2.643 GHz, 0.843 GHz, and 0.997 GHz. The input signal is acquired with 4 different sampling frequencies, with average sampling rate of about 1Gsps. The aliased spectrum is shown in Fig. 11. We use 400 samples and the algorithm proposed in the last section to detect the frequency support of the three active bands. The mean-subtracted and normalized spectra of each sample set around the frequency support of the first detected active band, which has a center frequency at 0.843 GHz, are shown in Fig. 12. As can be seen from Fig. 12, the spectra of sample set 1 and sample set 2 have multiple overlapped active bands, while sample set 3 and sample set 4 have the correct spectra. To

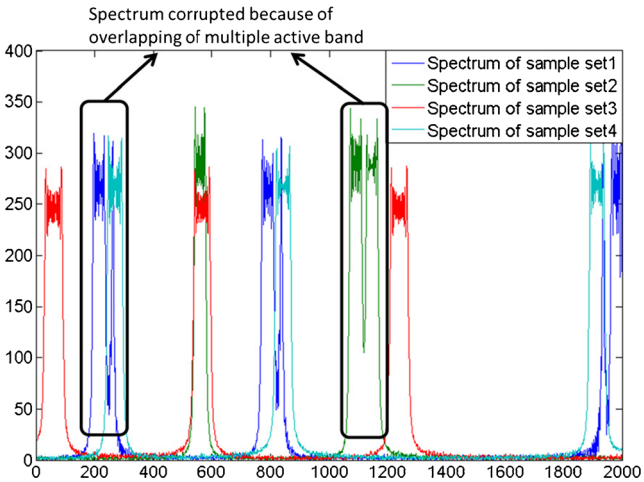

Fig. 11 Aliased spectrum of 4 different sampling sets

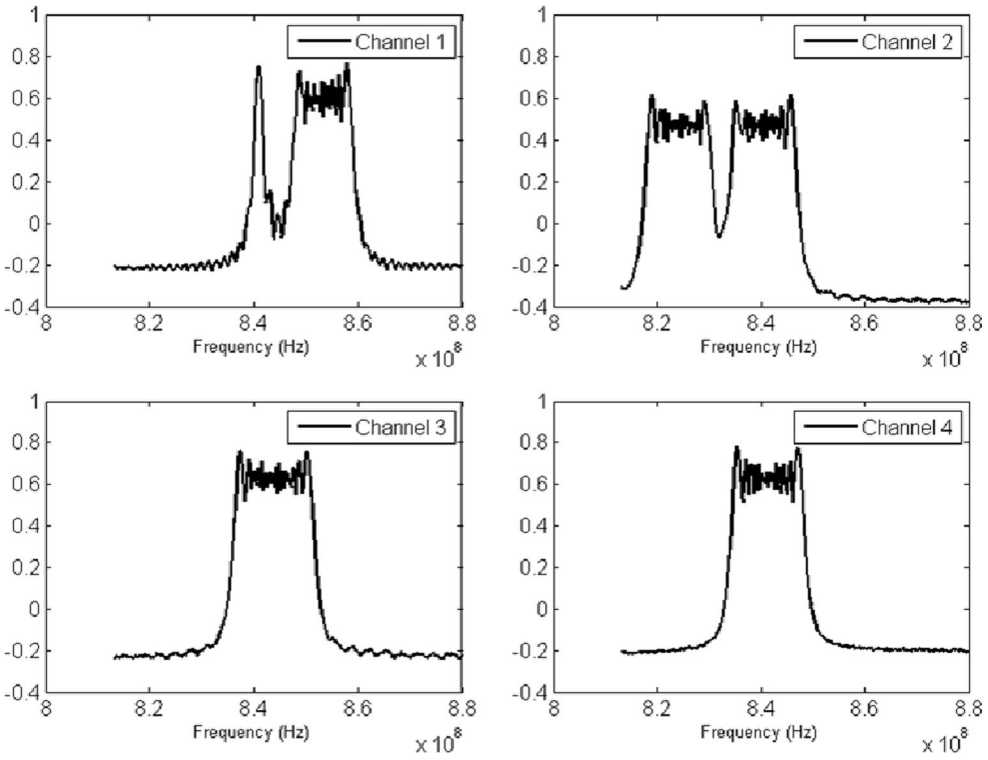

Fig. 12 Aliasing Spectra of different sets for the first active band

identify the correct spectra, we cross-correlate the spectra of different sample sets. The correct spectra will have higher correlation, while the spectra with multiple overlapped active bands will have low correlation with all other spectra. Therefore, we choose the two sample sets with highest spectra cross-correlation as the correct sample sets to use for characterization. Table 1 shows the cross-correlation of the spectra of the first active band. Sample set 3 and sample set 4 have the highest cross-correlation, as shown in the colored box. To further choose one sample set between sample sets 3 and 4, we use total variation (TV) as a metric [25] to select the smoother spectrum for characterization. The total variation of the spectrum of each sample set is shown in Table 2. Between sample sets 3 and 4, sample set 4 has the smoother spectrum, and thus smaller total variation. Choosing the metric is a design choice. For example, in [21], the total energy of the frequency support is used as the metric of choice. Once we identify one sample set, we can use an orthogonal spectral basis, instead of the common frequency grid, corresponding to the sampling frequency, to reconstruct the spectrum of the active band. For each active band, we use the same method to identify two correct spectra and choose one with total variation metric for characterization. The spectral reconstructions of different active bands are shown in Fig. 13.

Table 1 Spectrum correlation matrix of the first active band in Fig. 4

Active band 1	Sample set 1	Sample set 2	Sample set 3	Sample set 4
Sample set 1	X	−5.65	13.65	6.20
Sample set 2	−5.65	X	13.37	18.01
Sample set 3	13.65	13.37	X	25.58
Sample set 4	6.20	18.01	25.58	X

3 Incoherent Asynchronous Multi-Rate Hardware Architecture Design

3.1 Hardware Design

The hardware design goal is to develop a low-cost, low-complexity, and scalable design to support the proposed multi-rate

Table 2 Total variation of the spectrum of the first active band in Fig. 4

Active band 1	Sample set 1	Sample set 2	Sample set 3	Sample set 4
TV	8.3640	8.8831	6.0089	5.8462

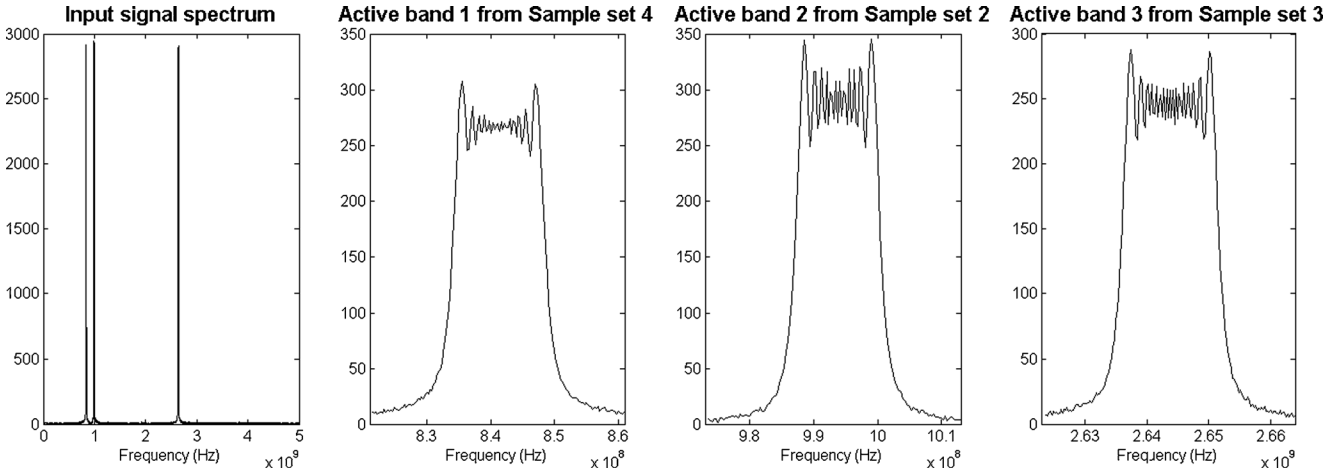

Fig. 13 The Input signal (*Left*), which contains 3 active bands, and 3 corresponding recovered active bands

signal acquisition algorithms. The options for sampling frequency are dictated by the programmable fractional frequency synthesizers used in the design. As shown in Fig. 14, a single multi-rate sampling module is capable of obtaining samples collected with different sampling frequencies. The single module can be scaled to multiple modules as in Fig. 15 for reduced signal acquisition time. The programmable frequency synthesizers in a multiple-module scheme can be different in order to increase the diversity of sampling rates. The input signal is split and fed into the wideband track-and-hold (T/H) amplifiers and digitized by identical analog-to-digital converters (ADCs). Since the hardware is intended to subsample wideband signals, the T/H amplifiers must have an input bandwidth that can support the bands to be sensed.

Multiple sampling frequencies are generated by a common clock base. Typically, a clean and low-frequency source is used as the clock base. The low frequency source is generated and fed into the second level PLLs, which then generate different sampling clocks for the ADCs and T/H amplifiers. The sampling phase of the ADCs relative to the T/H amplifiers should be adjusted so that data acquisition is aligned with the hold phase of the T/H amplifier. The configuration for delay adjustment can be obtained by performing a one-time calibration. The calibration is performed by sending a high-frequency tone as an input signal and sweeping the phase difference between the ADC and T/H amplifier. The phase difference can be adjusted with the delay settings in the ADCs or additional adjustable delay chips. The ideal delay setting should be the one corresponding to the smallest signal attenuation. Typically, a range of delay settings result in the smallest attenuation, with the center of the range selected as the optimal delay setting. The range is about 200 picoseconds in our calibration. Because of this range of the delay setting, the system is more resilient to other factors that cause delay variation such as temperature. When the frequencies of sampling clocks are changed, the phase difference should be readjusted. The delay configuration for different sampling frequencies can be obtained by a one-time calibration, and the configuration can be stored and applied when the sampling clock is changed.

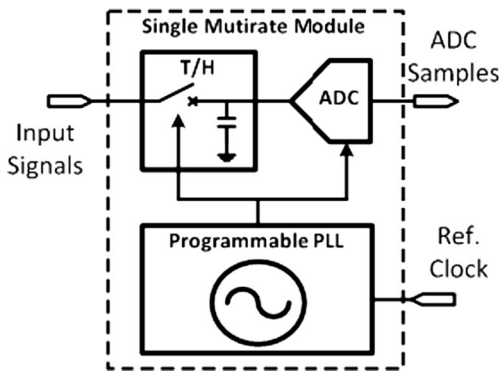

Fig. 14 Single Multi-rate Module

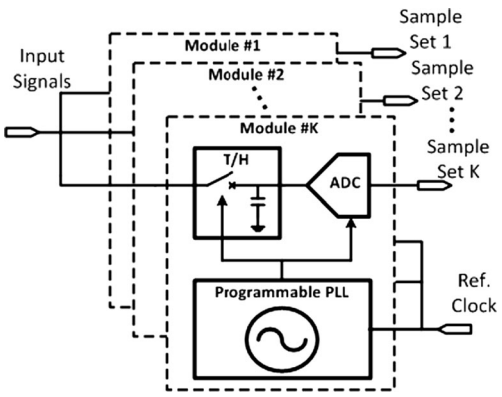

Fig. 15 Multiple Multi-rate Modules

3.2 Choosing Sampling Frequencies

A very commonly asked question is that of selecting the sampling frequencies in a multi-rate system. In general, choosing high sampling frequencies can reduce the possibility of active band overlapping and increase the algorithm performance. In addition, if one sampling frequency is an integer multiple of another sampling frequency, there will be no benefit. For example, a sample set with a sampling frequency of 500 MHz does not contribute any information if there is already another sample set with a sampling frequency of 1 GHz. In fact, the limitation here comes from the hardware implementation. Current high-end signal generators can generate clean single-tone signals at micro-Hz resolution and the signals can serve as clean sampling clocks in multi-rate systems. This means that almost any sampling frequency can be obtained with expensive high-end equipment. To simplify the system complexity and component cost, single-chip programmable PLLs are used to generate the sampling clocks. These single-chip PLLs can only generate a few different frequencies depending on their individual designs. The options for sampling frequencies are thus limited by the PLLs used. Simulation experiments have shown that for similar sampling frequencies, the performance in terms of recovery success rate does not vary much with different sampling frequencies. Since we do not make any assumption with respect to the input signal except that it has a sparse spectrum, the sampling frequencies are randomly chosen around the highest capable frequencies of the PLLs. In our hardware prototype, we use TI LMX2541 frequency synthesizers to generate the sampling clock. The options for generated output frequency depend on the two frequency dividers. To generate frequencies within a similar range (around 1GHz), we use two devices from the LMX2541 family but with different part numbers to increase the diversity of sampling frequency options.

3.3 Comparison with Other Sub-Nyquist Sampling Schemes

If we compare the proposed hardware scheme to other sub-Nyquist sampling schemes, the calibration requirements and system imperfections caused by hardware non-ideality and variations are significantly alleviated by our proposed signal acquisition approach. There are two required calibration steps in our work. As with other signal acquisition systems, each channel's path loss needs to be calibrated. Second, the delay between the track-and-hold circuitry and the ADC at different sampling frequencies is calibrated to ensure the integrity of the sampled signal. A table comparing the pros and cons of our approach vs. other methods is shown in Table 3. The key advantage of the proposed approach is that the effort required for measurement calibration is relatively low compared to the effort required for other synchronous and mixer-based systems. A hardware prototype can be implemented using all

Table 3 Hardware implementation comparison

Reference	[17]	[16]	[9]	[27]	This work
Scheme	Modulated wideband converter	Multi-coset sampling (Periodic non-uniform)	Asychmous Multi-rate sampling	Non-uniform sampling	Asynchronous multi-rate sampling
Hardware prototype	All electrical	N/A	Electrical and optical	All-electrical	All electrical
Input bandwidth	2 GHz	N/A	18 GHz	2GHz	18 GHz
Scalability	Low	Low	Low (requiring redesign the optical components)	Low	High
Calibration & Comment	• Gain loss • Phase and amplitude of tones of periodic digital sequence • Low-pass filter characterization • Mixer characterization and calibration • Delay synchronization across different channels	• Gain loss • Delay synchronization across different channels • Delay between T/H and ADC (if T/H is used to increase ADC input bandwidth)	• Gain loss • Optical components are used to modulate and multiplex signals	• Gain loss • Delay between T/H and ADC • Sampling rate limited by ADC sampling rate. (Sampling rate May exceed ADC sampling rate with multi-channel scheme.)	• Gain loss • Delay between T/H and ADC

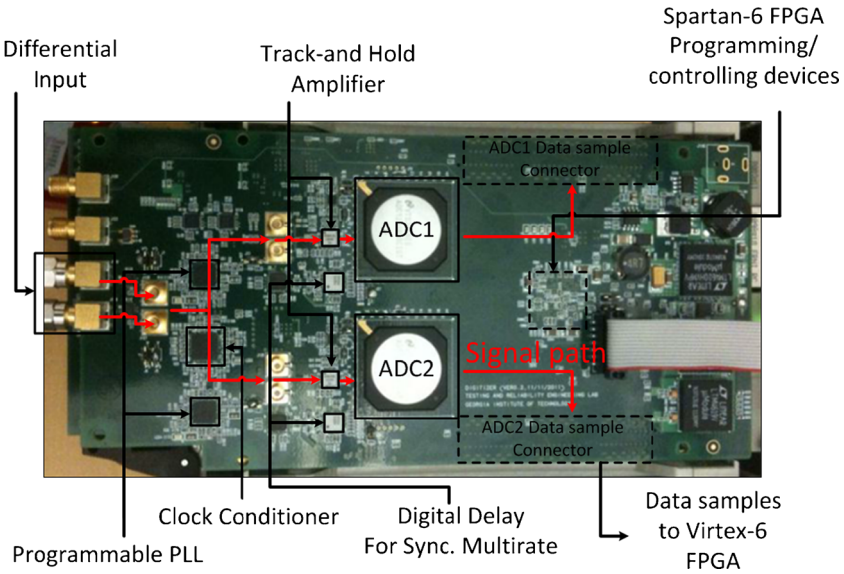

Fig. 16 Hardware prototype of the proposed design

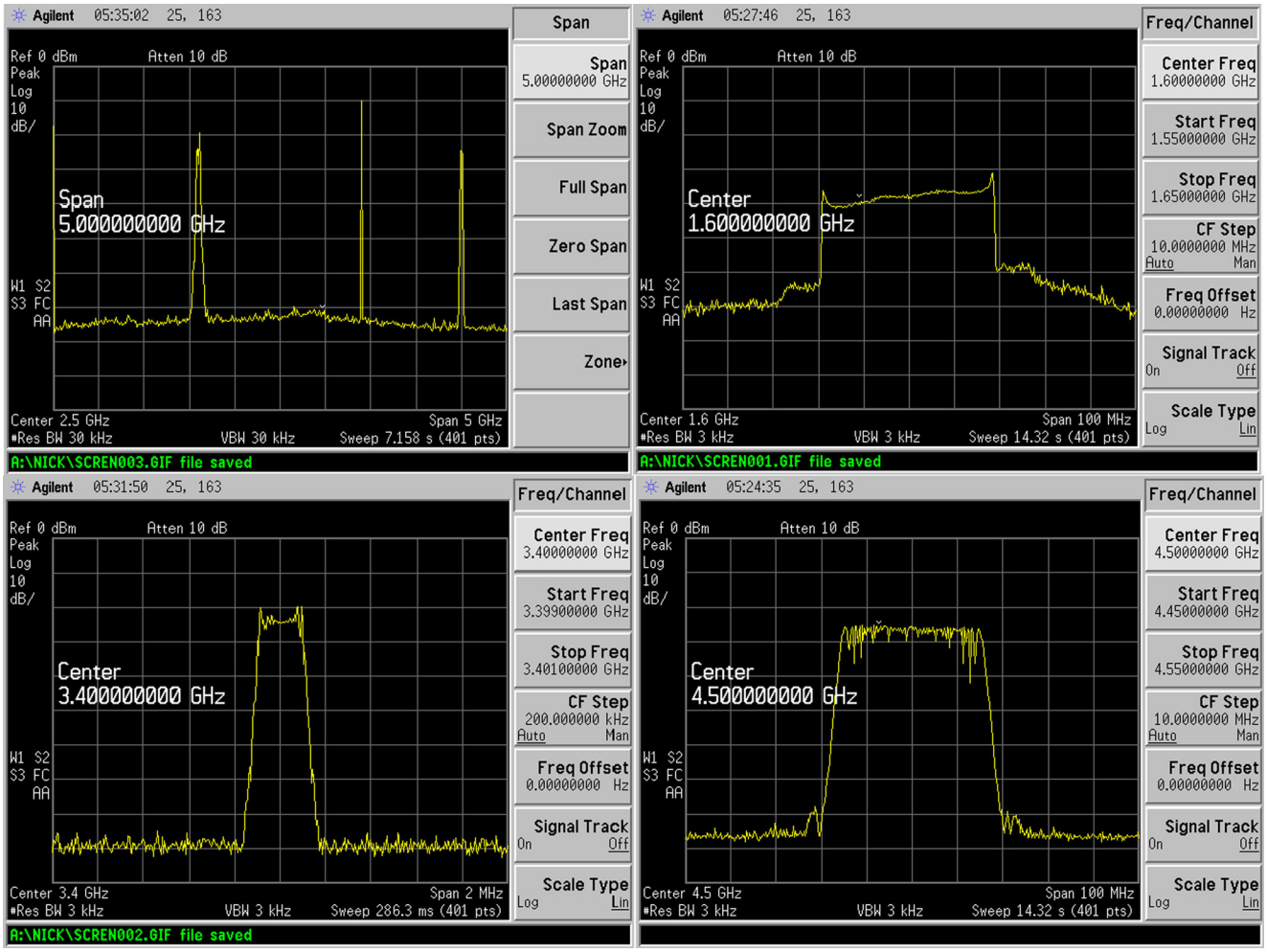

Fig. 17 The spectrum of the input signal (*Top left*) and three active bands

Table 4 Spectrum correlation matrix of the first active band

Active band 1	Sample set 1	Sample set 2	Sample set 3	Sample set 4
Sample set 1	X	19.20	−1.70	−0.37
Sample set 2	19.20	X	−0.83	−1.54
Sample set 3	−1.70	−0.83	X	15.01
Sample set 4	−0.37	−1.54	15.01	X

Table 5 Total variation of the spectrum of the first active band

Active band 1	Sample set 1	Sample set 2	Sample set 3	Sample set 4
TV	20.01	14.95	11.29	14.35

off-the-shelf components. Optical components or custom designed circuitry is not needed.

4 Hardware Measurement

We built a multi-rate system with electrical components based on the architecture proposed in Section III to serve as a prototype. Although it is difficult to scale up a synchronous multi-rate system, both synchronous and asynchronous algorithms can run using a synchronous multi-rate sampling scheme. Therefore, we built a synchronous multi-rate system for concept validation purposes. As shown in Fig. 16, the input signal is split into two channels that are directly fed to a Hittite 18 GHz wideband track-and-hold amplifier HMC5640BLC4B and a Hittite 5 GHz wideband track-and-hold amplifier HMC5641BLC4B. As mentioned in the previous section, these two track-and-hold amplifiers are used to increase the input bandwidth of ADCs for subsampling purposes. Since the two paths are different, we need to compensate for any gain difference between these two paths with a one-time frequency sweep calibration. In addition, for input bandwidths greater than 5 GHz, we can use only the channel with the 18 GHz T/H amplifier. Two ADC12D1800 ADCs are used to digitize signals after the 5-GHz and 18-GHz T/H amplifiers. The samples are then captured with a Xilinx Vertex-6 field programmable gate array for further processing.

Clock generation is critical in a multi-rate system. The system clock is fed to a clock conditioner LMK04033 to generate a clean low-frequency clock base. Texas Instruments LMX2541 synthesizers use this clock base to further generate the two different clocks for each channel. The track-and-hold and ADC of each channel takes its clock source from one of the two frequency synthesizers to acquire the data. The ADC's internal programmable aperture delay is set so the ADC samples at the hold phase of the track-and-hold amplifier. Since it is a synchronous multi-rate system, additional digital delay chips are required to adjust the delay between the two channels. A Xilinx FPGA Spartan-6 is used to program and control all the components, including the ADCs, digital delays, and frequency synthesizers.

Agilent E4423B, HP 8648D, and Agilent E8257D signal generators are used to generate three frequency-modulated signals which are combined to generate the input to the signal acquisition system. The center frequencies of the three frequency modulated signals are 1.6 GHz, 3.4 GHz, and 4.5 GHz, and the bandwidths are 60 MHz, 4 MHz, and 50 MHz respectively. The signals are combined and fed into the AMRS system. The spectra of these three active bands are shown in Fig. 17. Four different sampling frequencies (1.15GHz, 1.167GHz, 1.2GHz, and 1.25GHz) are used to capture the input signal. 16,384 samples are

Table 7 Total variation of the spectrum of the second active band

Active band 2	Sample set 1	Sample set 2	Sample set 3	Sample set 4
TV	3.25	2.45	2.55	14.08

Table 6 Spectrum correlation matrix of the second active band

Active band 2	Sample set 1	Sample set 2	Sample set 3	Sample set 4
Sample set 1	X	0.46	0.34	0.78
Sample set 2	0.46	X	1.14	1.02
Sample set 3	0.34	1.14	X	0.87
Sample set 4	0.78	1.02	0.87	X

Table 8 Spectrum correlation matrix of the third active band

Active band 3	Sample set 1	Sample set 2	Sample set 3	Sample set 4
Sample set 1	X	45.01	39.32	43.41
Sample set 2	45.01	X	40.44	43.68
Sample set 3	39.32	40.44	X	39.32
Sample set 4	43.41	43.68	39.32	X

Table 9 Total variation of the spectrum of the third active band

Active band 3	Sample set 1	Sample set 2	Sample set 3	Sample set 4
TV	91.70	92.00	98.82	88.80

acquired. The first 400 samples are used for active band detection. $(M = 400, N = 3000, B = 5\,GHz)$ Therefore, the spectral resolution with 400 samples is around 12.5 MHz (5 GHz / 400). Since the actual bandwidth is greater (60MHz>12.5MHz), a rectangular window of 60 MHz is convolved with the spectra to find the center of the active band. After the active bands have been correctly detected, the correlation matrix and the total variation metric is used to select the most representative spectrum of each active band to characterize the spectrum. Comparing the spectral shape of the active bands requires higher resolution. Therefore, 16,384 samples are used to perform spectrum classification and characterization. Tables 4, 5, 6, 7, 8 and 9 show the correlation matrices and total variations used to select sample sets for signal reconstruction. Sample set 1 is selected to characterize active band 3. Sample set 2 is selected to characterize active band 1 and active band 2. Orthogonal Fourier matrices are constructed with the sampling frequencies of the selected sample sets and used for characterization. The reconstructed spectra are shown in Fig. 18. Active band 2 has narrow bandwidth (2 MHz) and larger numbers of samples are needed to characterize such narrow band signals. The spacing of the Discrete Fourier spectrum is the sampling frequency divided by the number of samples. The resolution can be increased with the number of samples used for characterization.

5 Conclusion

In this paper we have proposed a low-cost and low-complexity sub-Nyquist signal acquisition hardware architecture and associated algorithms based on an asynchronous multi-rate sampling scheme. A hardware prototype is implemented with all off-the-shelf components to verify the proposed sampling scheme and algorithms.

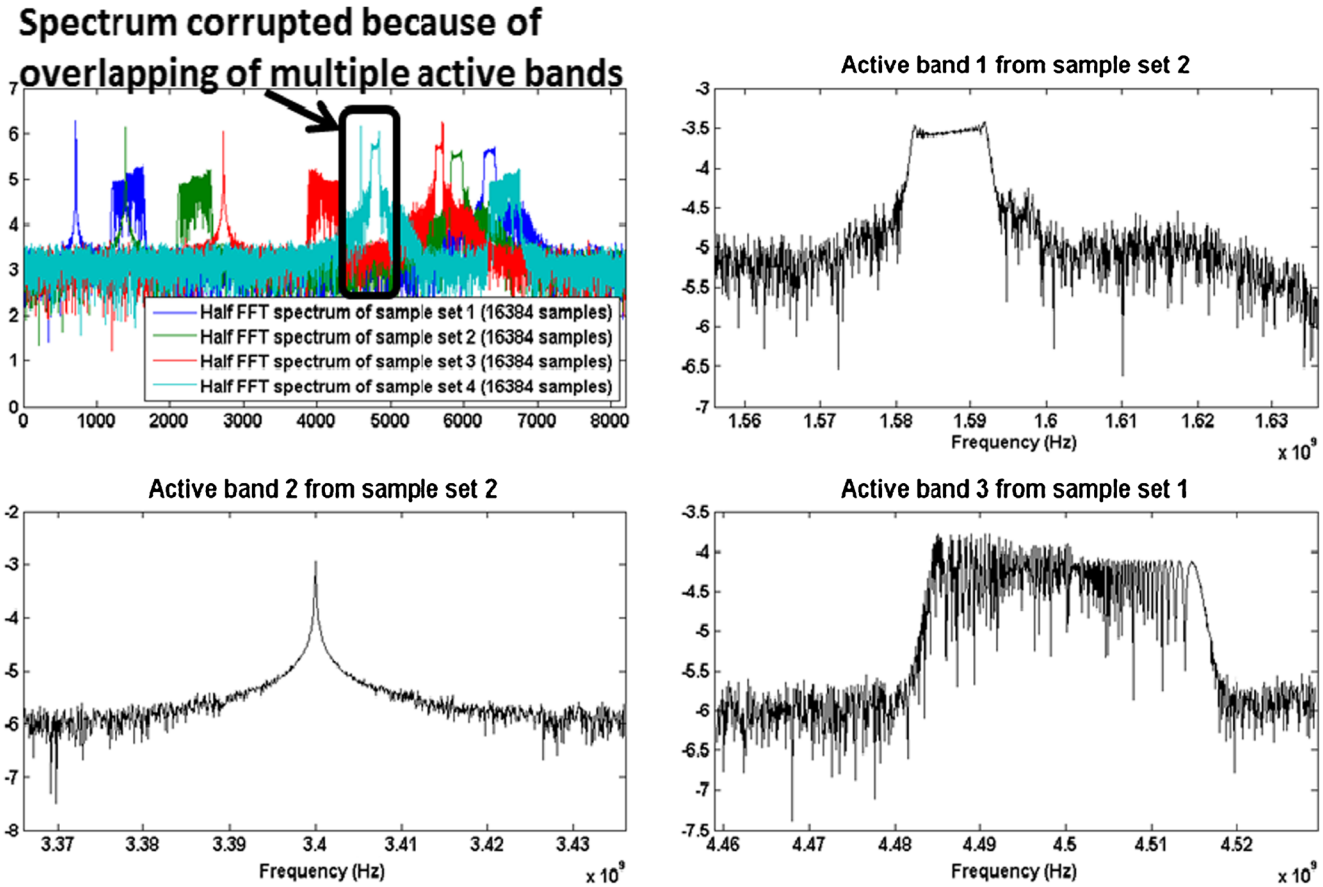

Fig. 18 Aliased spectrum of 4 different sampling sets (*Top left*) and the recovered spectrums

Acknowledgments The authors would like to thank Hittite Microwave for supporting this research by supplying components for the hardware prototype.

References

1. Babu DVS, Reddy PC (2012) Advancements of multi-rate signal processing for wireless communication networks: current state of the art. Glob J Comput Sci Technol 12(13-E).
2. Bresler Y, Ping F (1996) Spectrum-blind minimum-rate sampling and reconstruction of 2-D multiband signals. Proc IEEE Int Conf Image Process 1:701–704
3. Candès EJ, Romberg J, Tao T (2006) Robust uncertainty principles: exact signal reconstruction from highly incomplete frequency information. IEEE Trans Inf Theory 52(2):489–509
4. Domınguez-Jiménez ME, González-Prelcic N (2012) Analysis and design of multi-rate synchronous sampling schemes for sparse multiband signals.
5. Donoho DL (2006) Compressed sensing. IEEE Trans Inf Theory 52(4):1289–1306
6. Elbornsson J, Fredrik G, Eklund J-E (2005) Blind equalization of time errors in a time-interleaved ADC system. IEEE Trans Signal Process 53(4):1413–1424
7. Eldar YC, Oppenheim AV (2000) Filterbank reconstruction of bandlimited signals from nonuniform and generalized samples. IEEE Trans Signal Process 48(10):2864–2875
8. Feldster A, Shapira YP, Horowitz M, Rosenthal A, Zach S, Singer L (2009) Optical under-sampling and reconstruction of several bandwidth-limited signals. J Lightwave Technol 27(8):1027–1033
9. Fleyer M, Horowitz M, Feldtser A, Smulakovsky V (2010) Multi-rate synchronous optical undersampling of several bandwidth-limited signals. Opt Express 18(16):16929–16945
10. Fleyer M, Linden A, Horowitz M, Rosenthal A (2010) Multi-rate synchronous sampling of sparse multiband signals. IEEE Trans Signal Process 58(3):1144–1156
11. Johansson H, Lowenborg P (2002) Reconstruction of nonuniformly sampled bandlimited signals by means of digital fractional delay filters. IEEE Trans Signal Process 50(11):2757–2767
12. Kirolos S et al. (2006) Analog-to-information conversion via random demodulation. 2006 I.E. Dallas/CAS Works Des Appl Integ Softw, IEEE.
13. Laska J, Kirolos S, Massoud Y, Baraniuk R, Gilbert A, Iwen M, Strauss M (2006) Random sampling for analog-to-information conversion of wideband signals. 2006 I.E. Dallas/CAS Works Des Appl Integ Softw. IEEE. (pp. 119-122).
14. Laska JN et al. (2007) Theory and implementation of an analog-to-information converter using random demodulation. 2007 I.E. Int Symp Circ Syst. 2007 I.E. ISCAS.
15. Lu YM, Minh ND (2008) A theory for sampling signals from a union of subspaces. IEEE Trans Signal Process 56(6):2334–2345
16. Mishali M, Eldar YC (2009) Blind multiband signal reconstruction: compressed sensing for analog signals. IEEE Trans Signal Process 57(3):993–1009
17. Mishali M, Eldar YC (2010) From theory to practice: sub-Nyquist sampling of sparse wideband analog signals. IEEE J Sel Top Sign Process 4(2):375–391
18. Mishali M, Eldar YC, Dounaevsky O, Shoshan E (2011) Xampling: analog to digital at sub-Nyquist rates. IET Circ Devices Syst 5(1):8–20
19. Pfetsch S et al. (2008) On the feasibility of hardware implementation of sub-nyquist random-sampling based analog-to-information conversion. 2008 I.E. Int Symp Circ Syst. 2008 I.E. ISCAS.
20. Ragheb T et al. (2008) A prototype hardware for random demodulation based compressive analog-to-digital conversion. 2008 I.E. 51st Midwest Symp Circ Syst. 2008 MWSCAS.
21. Rosenthal A, Linden A, Horowitz M (2008) Multi-rate asynchronous sampling of sparse multiband signals. JOSA A 25(9):2320–2330
22. Sun H, Nallanathan A, Jiang J, Wang CX (2013) Multi-rate sub-Nyquist spectrum sensing in cognitive radios. arXiv preprint arXiv: 1302.1489.
23. Tian Z, Giannakis GB (2007) Compressed sensing for wideband cognitive radios. IEEE Int Conf Acoust Speech Signal Process. 2007 I.E. ICASSP 4.
24. Tropp JA, Gilbert AC (2007) Signal recovery from random measurements via orthogonal matching pursuit. IEEE Trans Inf Theory 53(12):4655–4666
25. Tzou N et al. (2012) Low-cost wideband periodic signal reconstruction using incoherent undersampling and back-end cost optimization. 2012 I.E. International Test Conference (ITC), IEEE.
26. Venkataramani R, Bresler Y (2001) Optimal sub-Nyquist nonuniform sampling and reconstruction for multiband signals. IEEE Trans Signal Process 49(10):2301–2313
27. Wakin M, Becker S, Nakamura E, Grant M, Sovero E, Ching D, Yoo J, Romberg J, Emami-Neyestanak A, Candes E A (2012)A nonuniform sampler for wideband spectrally-sparse environments. IEEE Journal on Emerging and Selected Topics in Circuits and Systems 2(3):516–529

Nicholas Tzou received B.S. degree in Electrical Engineering from National Taiwan University, Taipei, Taiwan, in 2009. He worked on his Ph.D. degree in Electrical and Computer Engineering at Georgia Institute of Technology, Atlanta from 2009 to 2014. He was a Research Assistant with the Testing and Reliability Engineering Lab, Georgia Institute of Technology since 2011. His research interest includes digital signal processing and wideband & high-speed signal characterization.

Debesh Bhatta received B.E. in Electronics and Telecommunication Engineering in 2005 from Jadavpur University, Kolkata, India. He received M.Tech. from Indian Institute of Technology, Kharagpur, India in 2007. He worked on his PhD at Georgia Institute of Technology, Atlanta, USA from 2007 to 2014. His research interests include high-speed analog circuit design and test.

Barry Muldrey (M'06) was born in New Orleans, Louisiana; he received his B.S. in electrical engineering from the University of New Orleans in 2009, and received his M.S. degree from the Georgia Institute of Technology in 2014. Since 2011, he has been conducting research at the Georgia Institute of Technology in pursuit of the Ph.D. degree. His work focuses on applied neural and machine learning with specific interest in their application to post-silicon validation, testing, diagnosis, and tuning, of mixed-signal systems. Barry is currently working under the supervision of Dr. Abhijit Chatterjee, and he has also enjoyed working for Drs. Jennifer Hasler and Douglas Williams. Barry also enjoys playing music, carpentry, and camping.

Thomas Moon received the B.S. degree in electrical electronic engineering from Pohang University of Science and Technology (POSTECH), Pohang, Korea, in 2008, and the M.S. degree in electrical and computer engineering from Georgia Institute of Technology, Atlanta, in 2012, where he is currently pursuing the Ph.D. degree. He is currently working as a Graduate Research Assistant with the Testing and Reliability Engineering Group, Georgia Institute of Technology. His current research interests include high-speed signal testing and characterization, signal integrity, and signal reconstruction by undersampling algorithm.

Xian Wang received the B.E. degree in electronic and communication engineering from City University of Hong Kong, Hong Kong, in 2010 and he is currently pursuing the Ph.D. degree in electrical engineering at Georgia Institute of Technology. From 2011 to present, he is a Research Assistant with the Testing and Reliability Engineering Lab, Georgia Institute of Technology.

Hyun Woo Choi (M'06) received the B.S. degree in electrical engineering from Korea University, Seoul, Korea, in 2004, and the Ph.D. degree in electrical and computer engineering from the Georgia Institute of Technology (Georgia Tech), Atlanta, GA, USA, in 2010.

Abhijit Chatterjee is a professor in the School of Electrical and Computer Engineering at Georgia Tech and a Fellow of the IEEE. He received his Ph.D in electrical and computer engineering from the University of Illinois at Urbana-Champaign in 1990. Dr. Chatterjee received the NSF Research Initiation Award in 1993 and the NSF CAREER Award in 1995. He has received six Best Paper Awards and three Best Paper Award nominations. His work on self-healing chips was featured as one of General Electric's key technical achievements in 1992 and was cited by the Wall Street Journal. In 1995, he was named a Collaborating Partner in NASA's New Millennium project. In 1996, he received the Outstanding Faculty for Research Award from the Georgia Tech Packaging Research Center, and in 2000, he received the Outstanding Faculty for Technology Transfer Award, also given by the Packaging Research Center. In 2007, his group received the Margarida Jacome Award for work on VIZOR: Virtually Zero Margin Adaptive RF from the Berkeley Gigascale Research Center (GSRC).